BIOCHEMISTRY
including biophysical chemistry & molecular biology

Article

pubs.acs.org/biochemistry

Distinguishing Amyloid Fibril Structures in Alzheimer's Disease (AD) by Two-Dimensional Ultraviolet (2DUV) Spectroscopy

A. R. Lam,* J. Jiang,* and S. Mukamel*

Department of Chemistry, University of California, Irvine, Irvine, California 92697-2025, United States

ABSTRACT: Understanding the aggregation mechanism of amyloid fibrils and characterizing their structures are important steps in the investigation of several neurodegenerative disorders associated with the misfolding of proteins. We report a simulation study of coherent two-dimensional chiral signals of three NMR structures of Aβ protein fibrils associated with Alzheimer's Disease, two models for Aβ(8−40) peptide wild-type (WT) and one for the Iowa (D23N) Aβ(15−40) mutant. Both far-ultraviolet (FUV) signals (λ = 190−250 nm), which originate from the backbone nπ^* and $\pi\pi^*$ transitions, and near-ultraviolet (NUV) signals ($\lambda \geq$ 250 nm) associated with aromatic side chains (Phe and Tyr) show distinct cross-peak patterns that can serve as novel signatures for the secondary structure.

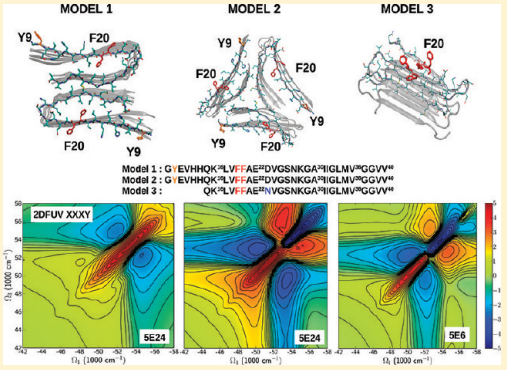

A large number of neurodegenerative diseases are linked to the formation and deposition of misfolded proteins to form amyloid fibrils. Probing the aggregation kinetics and fibril formation pathways had drawn a considerable experimental and computational attention.[1−14] Alzheimer's Disease (AD) is a progressive neurodegenerative disorder whose pathology is characterized by the accumulation of senile plaques and neurofibrillar tangles in the brain. These plaques are made of fibrillar aggregates of the amyloid β-protein (Aβ). This protein comes from the cleavage of the amyloid precursor protein (APP) and is present in the body predominantly in two alloforms: Aβ40, and Aβ42, which has two additional amino acids in the C-terminal.[15,16]

Determination of the structure of amyloid fibrils is a challenging task. X-ray diffraction is a common tool used for the determination of global atomistic structures of proteins in crystals, whereas nuclear magnetic resonance (NMR) techniques can yield structures in solution. The information obtained from these conventional structural biology techniques is limited because amyloid fibrils are insoluble and do not crystallize. High-resolution molecular structure of amyloid fibrils is not available, but geometrical models based on solid NMR and other experimental data have been proposed.[17−20] Recent CD and NMR studies of Aβ monomers and dimers in solutions were used to characterize global properties such as secondary structures at different concentrations, pH, and temperatures.[11,21,22] Ultraviolet (UV) spectroscopy provides an alternative structural tool. Both the peptide backbone and aromatic side chains are active in this regime. The nπ^* and $\pi\pi^*$ backbone transitions in the far-ultraviolet (FUV) region (λ = 190−250 nm) are used for estimating secondary structure content. Circular dichroism (CD) spectroscopy in this region is a useful probe for secondary structures than can distinguish between α-helices and β-strands. In the near-ultraviolet (NUV) region ($\lambda \geq$ 250 nm), aromatic side chains (Phe, Tyr, and Trp) provide more details about local interactions. Absorption and CD spectra of proteins are usually calculated using the Frenkel exciton matrix model, which provides an efficient parametrization scheme for their electronic excitations.[23−27]

Two-dimensional (2D) optical spectroscopy is a novel tool that can be used for structure refinement. Sequences of femtosecond laser pulses are employed to excite vibrational or electronic states and determine correlations between events that occur within two controlled time intervals. These correlations are displayed in two-dimensional maps that reveal the molecular motions and fluctuating structures of a protein. These could help characterize local dynamics and determine intermediate states in the Aβ fibril formation process.[28−31] Two-dimensional infrared (2DIR) photon echo experiments combined with molecular dynamics simulations (MD) have been employed to test the quality of the MD methods and probe protein structures and fast folding processes. Previous simulation studies have demonstrated the potential of two-dimensional ultraviolet spectroscopy (2DUV) in the FUV and NUV regions for characterizing the secondary structure of Aβ amyloids. A simulation protocol based on the Exciton Hamiltonian with Electrostatic Fluctuations (EHEF) was developed.[32−34] The present computational study employs that protocol and is aimed at demonstrating how the cross-peaks in chiral 2DUV signals may be used to distinguish between three Aβ amyloid fibril geometrical models suggested recently by the NMR studies of Tycko and co-workers.[17−20]

Received: August 19, 2011
Revised: September 29, 2011
Published: September 30, 2011

In the Materials and Methods section, we explain the EHEF protocol, provide some technical details and present the amyloid fibril models used. In the Results and Discussion section, we present the simulated one- and two-dimensional NUV and FUV spectra. Finally, we provide the Conclusions.

MATERIALS AND METHODS

We consider the three Aβ peptides models shown in Figure 1. Models 1 and 2 correspond to the Aβ(8−40) peptide with the sequence GYEVHHQK^{16}LVFFAE^{22}DVGSNKGA^{30}IIGLMV^{36}GGVV^{40}. Model 1, first suggested by Petkova et al.,[18] consists of parallel β-sheets growing along the fibril growth axis. Model 2, which has a three-fold symmetry about that axis, is based on solid-state NMR and electron microscopy performed by Paravastu et al.[19] We used three peptides in each block, making a three-fold symmetry complex composed of nine peptides. Model 3 is the Aβ(15−40) segment of the above protein with the point D23N mutation, known as the Iowa mutant. Its geometry consists of an antiparallel β-sheet growing along the fibril axis.[20]

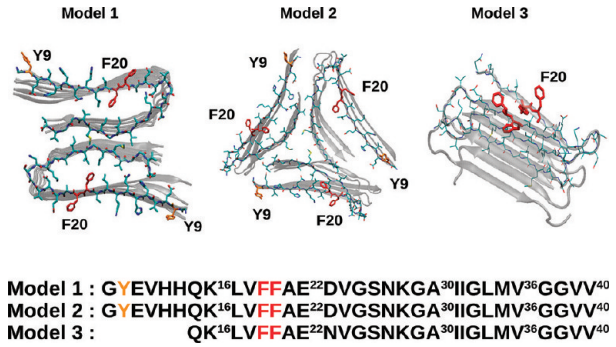

Figure 1. Structure and sequence of the three Aβ amyloid fibril models reported by Tycko and co-workers.[18−20] The aromatic residues are marked: phenylalanine (red) and tyrosine (orange).

MD trajectories of the above models were obtained by using the NAMD Package 2.7[35] with the CHARMM27 force field.[36] Simulations were carried out in aqueous solutions with TIP3P water and cubic periodic boundary conditions. The particle-mesh Ewald (PME) protocol was used to calculate the long-range electrostatic interactions, and a 12 Å cutoff distance was used for nonbonded interactions. The 2.0 ns runs were used to minimize the proteins at 300 K, and 1250 MD snapshots were subsequently harvested for the 2DUV calculations. Made using the EHEF protocol[32−34,37] and the SPECTRON homemade program.[38]

The simulated linear absorption (LA) and CD spectra in the entire UV regime (λ = 180−250 nm) for the three models are displayed in Figures 2 and 3, respectively. We show the spectra of the side chain alone (black), the backbone (red), the additive spectrum (their sum, blue), and the total spectrum (green). The difference of the additive and the total spectrum shown in the right column in Figures 2 and 3 is a measure of interactions between the backbone and side chains. The strongest differences are around 52000 cm^{-1}. The NUV region (above 250 nm) covers transitions of aromatic side chains (Phe, Tyr, and Trp). Each has four valence electronic excitations known in

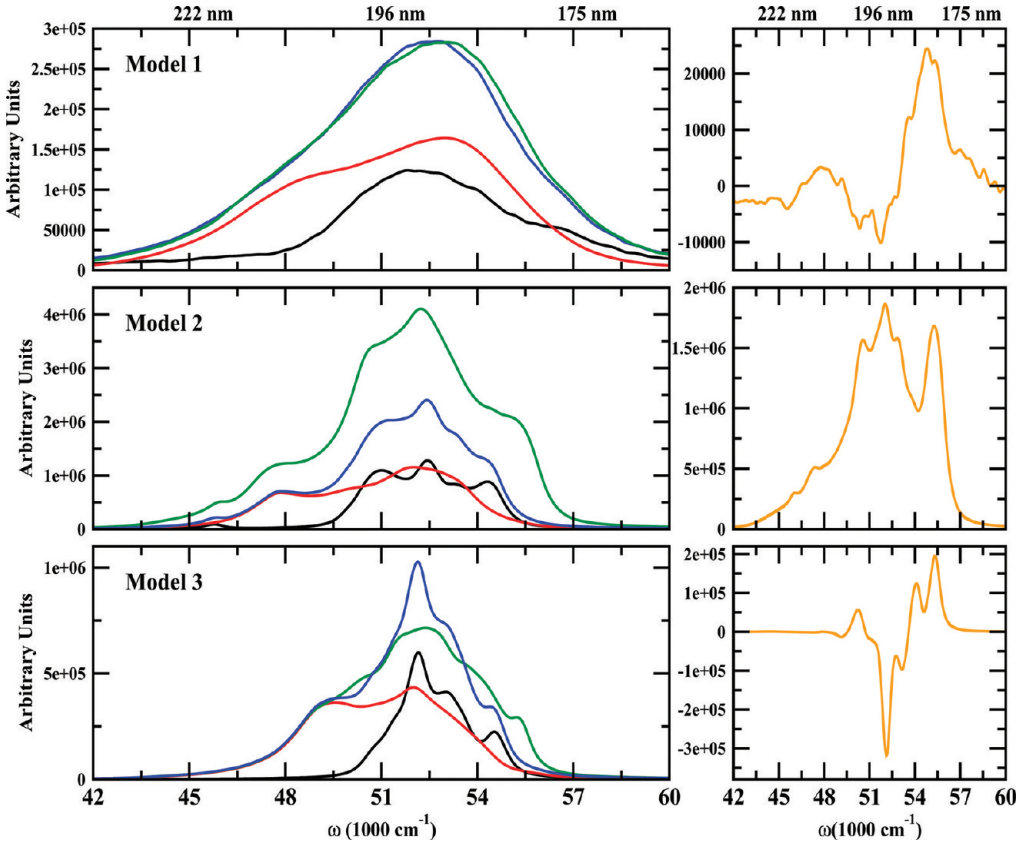

Figure 2. Left column: Simulated LA spectra. Total signal (green), backbone alone (red), side chain alone (black), additive spectrum (backbone + side chain) (blue). Right column: Difference of the total and the additive LA spectra (orange).

dx.doi.org/10.1021/bi201317c | Biochemistry 2011, 50, 9809−9816

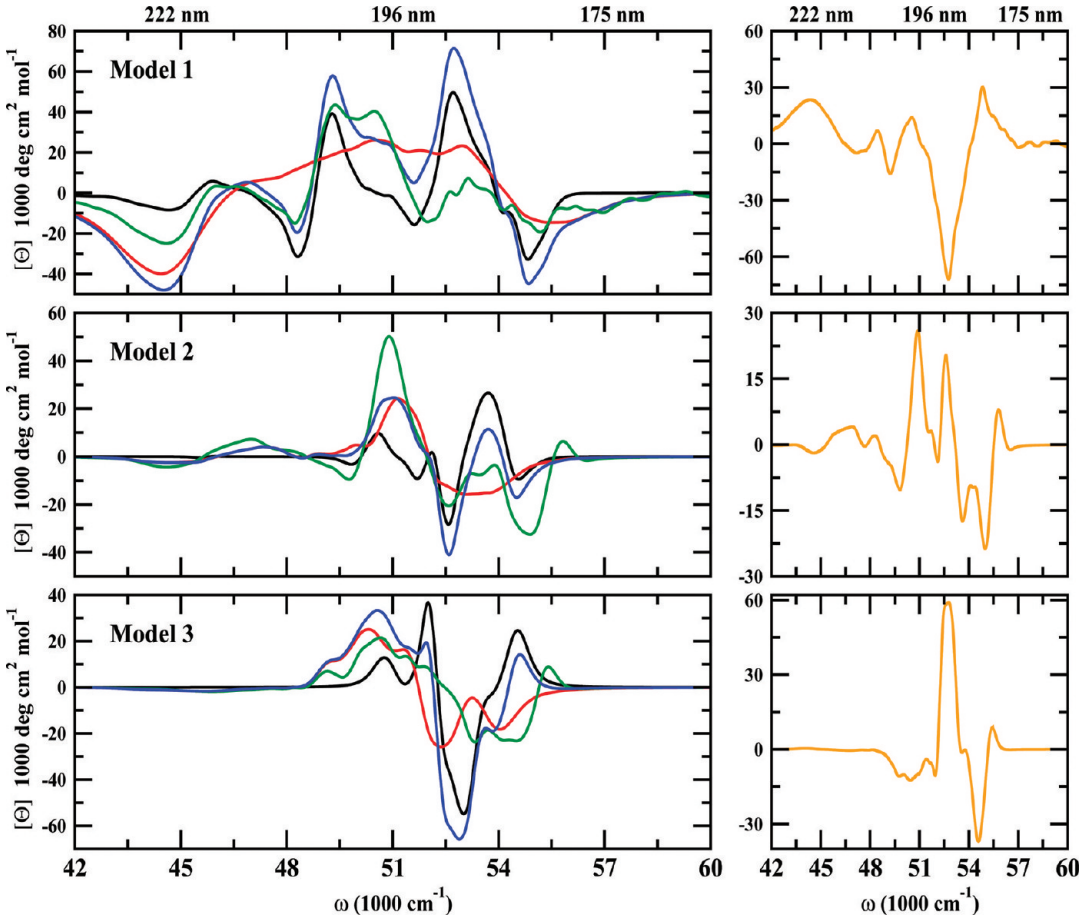

Figure 3. Same as in Figure 2 but for the CD spectra.

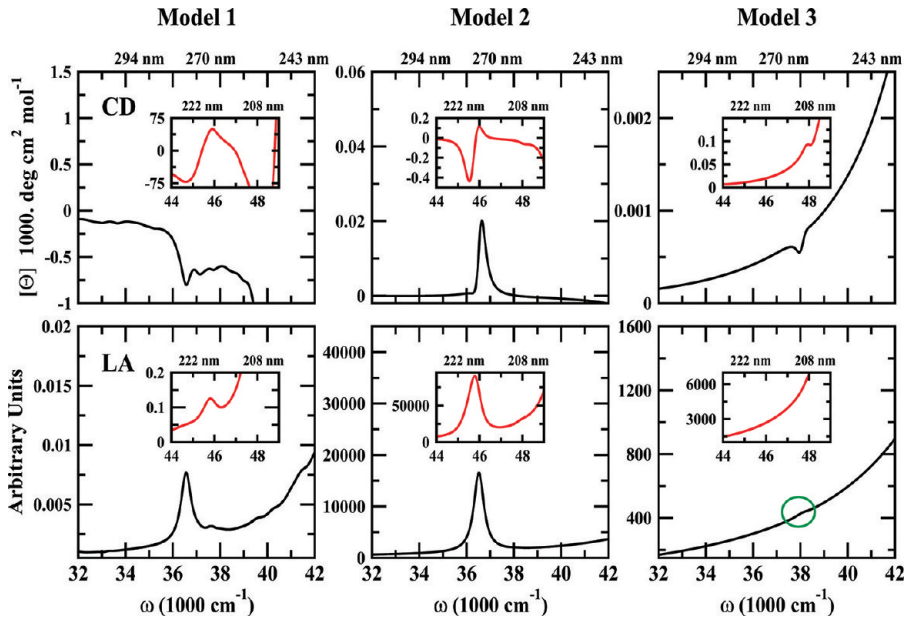

Figure 4. Simulated NUV CD (top row) and LA (bottom row) of the three Aβ amyloid models. Insets show the region [44000, 48000] cm^{-1}.

Platt's notation as ^1L_a, ^1L_b, ^1B_a, and ^1B_b. ^1L_a and ^1L_b give the strong NUV peaks. The interactions of the aromatic residues may be used to characterize the structure. NUV signals of model 1 were reported earlier.[34,37] The FUV spectra (190−250 nm) originate from the peptide backbone nπ^* and $\pi\pi^*$ transitions and are also sensitive to secondary structure. Even though aromatic residues are rare (three out of twenty residues), their contributions to the FUV spectra are not much weaker than those of the backbone because they have larger transition dipole moments. The difference spectrum is

dx.doi.org/10.1021/bi201317c | *Biochemistry* 2011, 50, 9809−9816

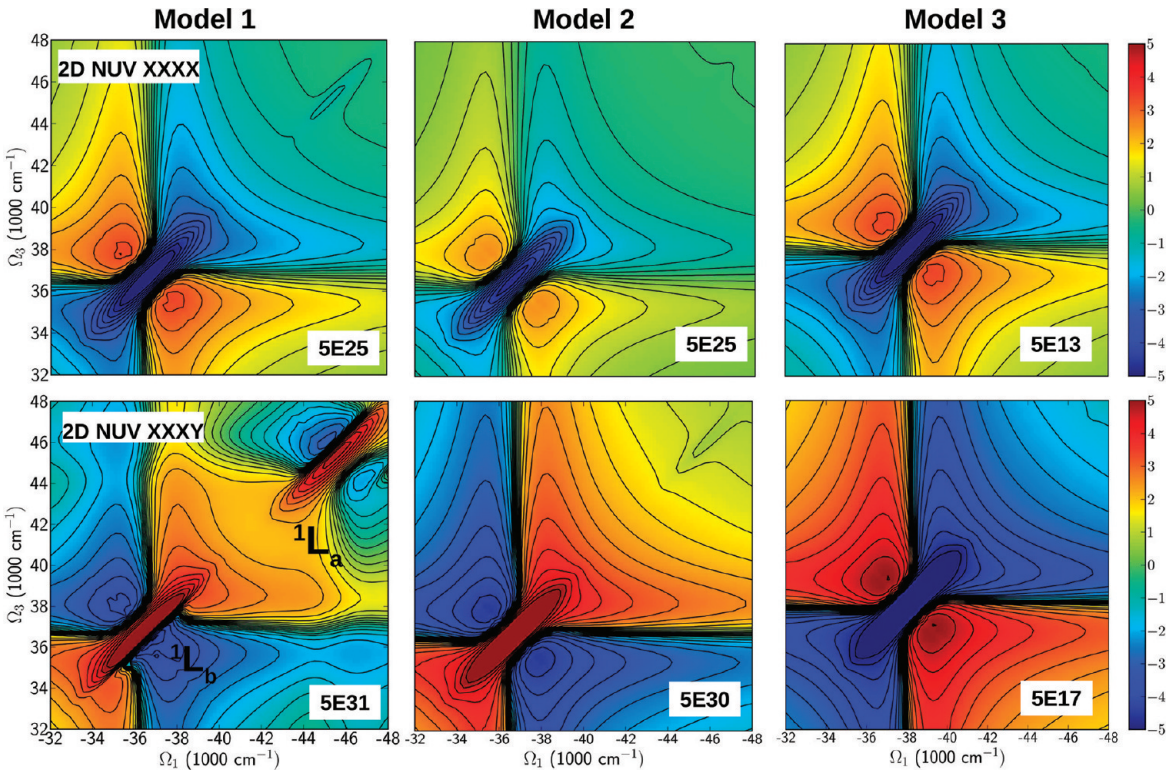

Figure 5. Simulated 2DNUV photon echo signals of the three Aβ amyloid models. Top row: The nonchiral (*xxxx*) polarization configuration. The signals show a similar pattern but different intensities. Peaks centered at 37000 cm^{-1} are similar in intensity for models 1 and 2, while in model 3, they are shifted away from the center and less intense. Bottom row: Chirality-induced (*xxxy*) polarization configuration. The spectra show some differences in the ^1L_b region (37000 cm^{-1}). Model 1 has a strong ^1L_a transition at 46000 cm^{-1}, while that in Model 2 is weaker. Spectra are displayed on the nonlinear scale as defined in ref 34. The *c* parameter is given at the bottom right of each panel.

much stronger for LA than for CD. The CD backbone spectra in all models (Figure 3, red plots) show a clear FUV signatures of a typical β-strand conformation.

In the coming sections, we shall analyze the NUV and FUV spectra in detail.

RESULTS AND DISCUSSION

Near-Ultraviolet (NUV) Signals. The simulated LA signals in the NUV regime for all three models are shown in Figure 4 (bottom). For models 1 and 2, they exhibit sharp peaks at around 37000 cm^{-1}, while model 3 only shows a modest bump (indicated by green circle) at 38000 cm^{-1}. Another peak is observed at 46000 cm^{-1} for models 1 and 2. This feature is missing in model 3 due to its shorter sequence that does not have the tyrosine (Tyr) Y9. We expect that a full sequence for model 3 should show aromatic side chain transitions at 46000 cm^{-1}.

The 2DNUV spectra computed with laser pulses centered at 37000 and with 3754 cm^{-1} bandwidths are displayed in Figure 5. All 2D spectra in this article are plotted on a nonlinear scale[34] that interpolates between logarithmic for small values and linear for large values and thus reveals both the strong and weak features. The nonchiral (*xxxx*) signals (all pulses have parallel polarization) are shown in the top row. For model 1, the signal is symmetric with respect to the diagonal. The ^1L_b transitions dominate and show a negative diagonal peak (blue) centered at 37000 cm^{-1}. This is accompanied by two positive (red) side bands. The ^1L_a transitions that originate from the coupling between the aromatic residues Phe and Tyr appear as a peak in model 1 at around 46000 cm^{-1} (blue), a weaker peak appears in model 2, and no peak is present in model 3, where ^1L_a transitions are invisible due to the lack of Tyr Y9. In models 2 and 3, the ^1L_b transitions shifted to 36000 cm^{-1} dominate with their respective side bands, but model 2 seems to have a weaker ^1L_b transition than models 1 and 3.

We next turn to chirality-induced (*xxxy*) signals. The CD spectra of all models shown in Figure 4 have aromatic side-chain peaks at 37000 and 46000 cm^{-1}. Model 3 also shows tiny peaks that could be attributed to an aromatic side-chain transition between a Phe of a peptide with the other Phe in another peptide on the same layer.

The chirality-induced (*xxxy*) 2DUV signal of model 1, where the last pulse is polarized perpendicular to the other three (bottom row in Figure 5), is nonsymmetric with respect to the diagonal. The ^1L_b and ^1L_a transitions appear as two positive (red) peaks with their negative side bands centered at around 37000 and 46000 cm^{-1}, respectively. The ^1L_b peak has a strong sideband in the lower triangle, shifted from the diagonal, while a similar pattern is seen in the upper sideband of the ^1L_a transition peak. This indicates that the ^1L_b and ^1L_a transitions are coupled. The signals of models 2 and 3 are very different from that of model 1. Both are symmetric but have different intensities. The ^1L_b transition of model 2 is stronger than that in model 3. This may be due to the nearest-neighbor interactions between Phe in the Aβ peptides in model 2 that exist also in model 1. ^1L_a is weak in models 2 and 3, suggesting weak coupling between ^1L_b and ^1L_a transitions. A possible explanation could be that Phe and Tyr interact with each other in one Aβ peptide in a given layer and generate a coupling between ^1L_b and ^1L_a transitions. The geometry of model 2

dx.doi.org/10.1021/bi201317c | *Biochemistry* 2011, 50, 9809–9816

allows Tyr to interact with the Phe of another Aβ peptide in a different layer. Our previous 2DNUV studies of the amyloid fibril growth in model 1[39] showed how the signals intensities correlate with the aggregate size. Intramolecular interaction of aromatic residues Phe-Tyr in one Aβ peptide is seen only in model 1, while aromatic residue couplings are missed in model 3, which lacks the Tyr residue (Y9) in its sequence.

In order to trace the origin of these spectral features, we have computed the transition populations. These are defined as the squares of the exciton wave function expansion coefficients in the basis of the local amide excitations and are displayed in Figure 6. We see that the NUV (*xxxy*) signals (bottom row in Figure 5) of all models are induced by the aromatic residues (Phe and Tyr) and are well localized in the sequence. In model 2, the ^1L_b transition is observed as a red peak in the 34000−36000 cm^{-1} region, but no couplings (perhaps very weak) between ^1L_b and ^1L_a transitions are observed in the 44000−46000 cm^{-1} region. Model 3 shows a blue peak in the 34000−36000 cm^{-1} region, while models 1 and 2 have red peaks that can be ascribed to the complex geometry because it has only Phe-Phe intermolecular interactions between two peptides. Similarly, the 44000−46000 cm^{-1} region shows signals for models 1 and 2 but not model 3.

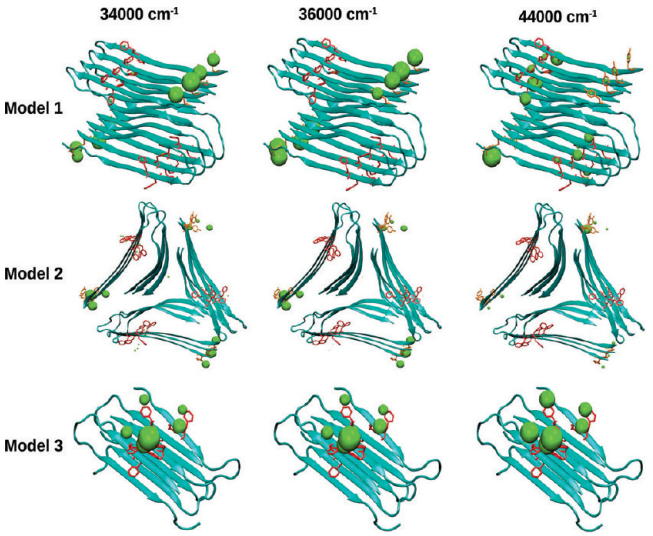

Figure 6. Transition populations for three NUV spectral regimes of the Aβ amyloid fibril models.

Far-Ultraviolet (FUV) Signals. The simulated LA and CD spectra of the three Aβ peptide amyloid fibril models in the FUV region shown in Figure 7 are similar with peaks centered at around 52000 cm^{-1}. The 2DFUV spectra generated by laser pulses centered at 52000 cm^{-1} and a bandwidth at 3754 cm^{-1} are displayed in Figure 8. The nonchiral 2DUV (*xxxx*) spectra (top row) show the characteristic features of a β-sheet, a weak peak centered at around 52000 cm^{-1} on the diagonal maps ($\Omega_3 = -\Omega_1$) for all three models.

We next turn to the chiral signals. The CD signals are distinguishable and have the characteristic of a β-strand rich-structure profile, in agreement with experiments.[21,22,40] Model 1 has stronger CD signals in the 50000−54000 cm^{-1} region, whereas signals for models 2 and 3 show peaks at around 50000 cm^{-1} and decay beyond 52000 cm^{-1}. The (*xxxy*) chiral 2DUV signals are much richer than the (*xxxx*) spectra (Figure 8, bottom row). Model 1 has a symmetric strong peak at 52000 cm^{-1}. Models 2 and 3 show a symmetric butterfly-like spectra with a positive peak near 52000 cm^{-1} and a negative peak at 54000 cm^{-1}. Model 3 has an additional positive peak near 57000 cm^{-1}. The transition populations in the FUV regime are displayed in Figure 9. These reveal that at 52000 cm^{-1}, the signals for all three models come from the electronic transition of all peptide groups and reflect the strongest peak of the CD spectra (see Figure 9 top row, left column). At 54000 cm^{-1}, weak contributions from the backbone are seen only in model 1 CD and LA spectra. In contrast, that region shows a broad feature that overlaps with the 52000 cm^{-1} peak (Figure 9 top

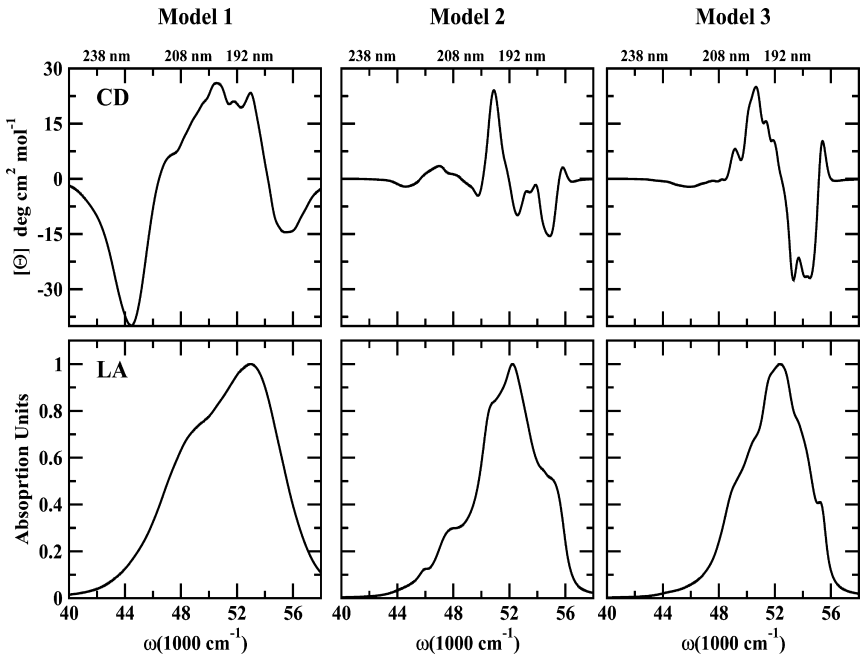

Figure 7. Simulated FUV CD (top row) and LA spectra (bottom row) of the three Aβ amyloid models.

dx.doi.org/10.1021/bi201317c | *Biochemistry* 2011, 50, 9809−9816

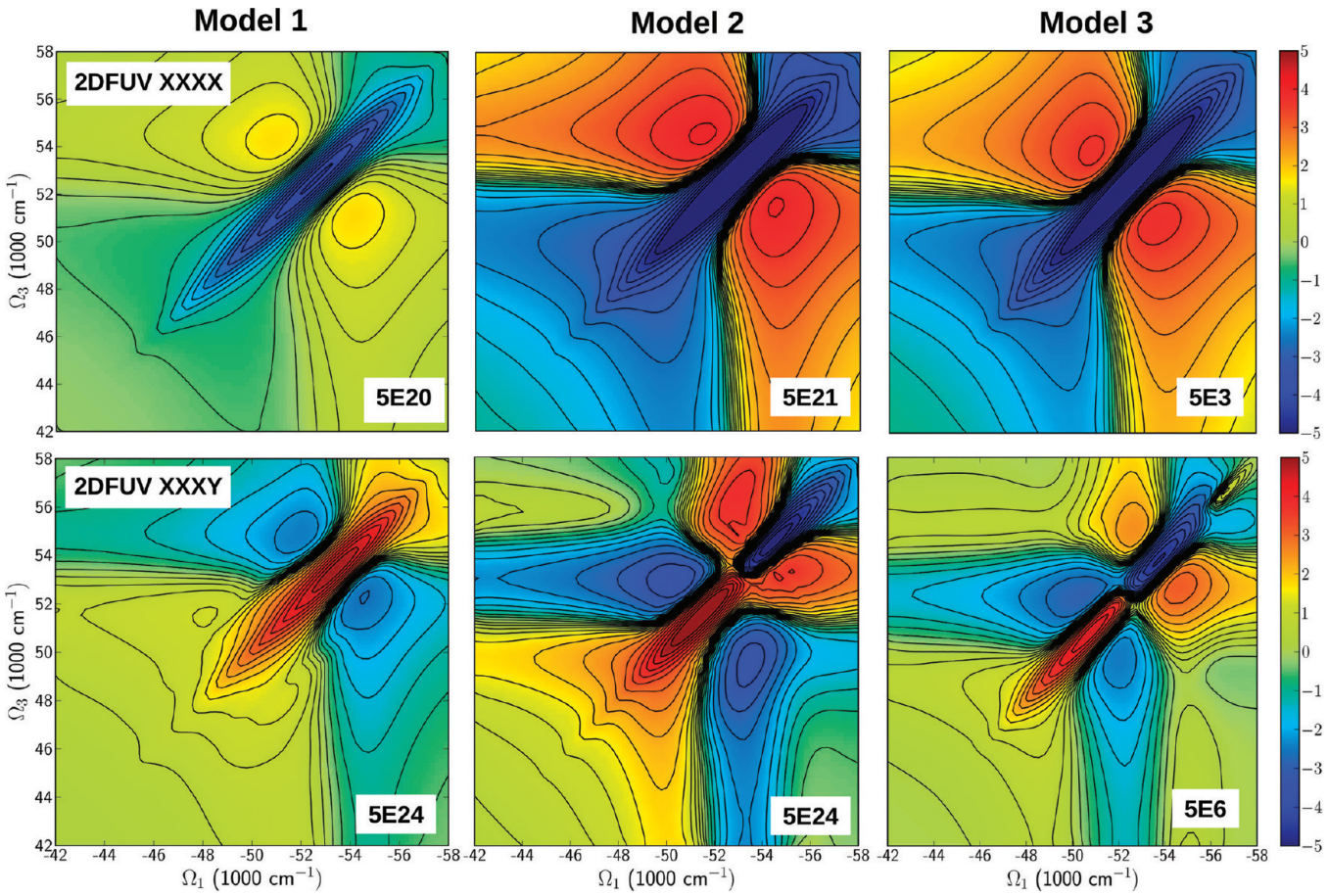

Figure 8. Same as in Figure 5 but for the 2DFUV regime. Top row: The nonchiral (*xxxx*) polarization configuration. All models display a similar pattern but different intensities. Bottom row: Chirality-induced (*xxxy*) polarization configuration. Model 1 has a strong peak at 52000 cm^{-1}, while models 2 and 3 show butterfly-like shapes with two peaks in the 50000−54000 cm^{-1} regime. Model 3 has a small additional peak at 57000 cm^{-1}.

row, left panel). The middle column in Figure 9 shows that this is mainly due to interactions between the turn loop of a Aβ peptide located in a β-sheet layer and the terminal of a Aβ peptide located in the other β-sheet layer. The 2DFUV signals of models 2 and 3 are different. They show an additional weak peak at 54000 cm^{-1} on the 2DFUV spectra originating from the interactions between turn-ends of different fibrils layers. The CD spectra of both models in the 52000 and 54000 cm^{-1} regions are different. We expect a similar 2DUV spectrum to those of models 1 and 3 because their global geometries consist of a β-sheet layer with alternate loops between Aβ peptides. However, the two show significant differences. The 2DFUV spectra (Figure 8 lower-right plot) shows also a butterfly-like spectrum as in model 2, indicating that in addition to the interactions between turns of a Aβ peptide from a β-sheet layer with the ends of a Aβ peptide from another β-sheet layer as in model 2, the complex geometry is important as well. Both models show interactions between turns and termini among peptides. In model 2, these are between stacks, while in model 3, they are among peptides in the same stack. This could account for the differences between the 2DFUV spectra.

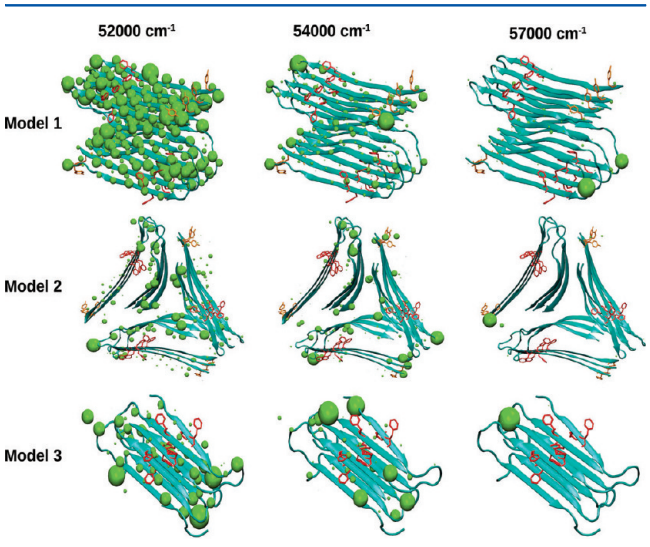

Figure 9. Transition populations for three FUV spectral regimes of the Aβ amyloid fibril models.

CONCLUSIONS

We have employed the EHEF protocol to predict the 2DUV spectra of three amyloid fibril structure models proposed by Tycko and collaborators. The 1D (CD and LA) spectra of the three models suggest that the side chains and backbone transitions are coupled. 2DUV spectra of the aromatic side chains show clear signatures of ^1L_b and ^1L_a transitions and their respective couplings in all models. The 2DFUV chirality-induced (*xxxy*) signals associated with aromatic residue couplings between transitions can describe the variations of

dx.doi.org/10.1021/bi201317c | *Biochemistry* 2011, 50, 9809−9816

interactions between residues, which strongly depend on the complex geometry. The ^1L_b and ^1L_a couplings can be hidden in the 2DFUV maps by either intermolecular interactions of aromatic residues Phe-Tyr as seen in model 2 or a correlation between the number of peptides in a Aβ sheet with the 2DUV intensity. Because the sequence of the Iowa mutant Aβ peptide shown in model 3 was shorter, the ^1L_b and ^1L_a transitions were undetectable. However, its geometry (peptides forming an antiparallel β-strand sheet) had resulted in butterfly-like chiral-induced signals in the FUV, similar to model 2.

AUTHOR INFORMATION

Corresponding Author

*E-mail: alamng@uci.edu (A.R.L.); jiang1@uci.edu (J.J.); smukamel@uci.edu (S.M.). Phone: +1 949-824-6164. Fax: +1 949-824-4759.

Funding

National Institutes of Health (Grant GM059230 and GM091364) and National Science Foundation (Grant CHE-1058791).

ACKNOWLEDGMENTS

We wish to thank Dr. Robert Tycko for providing the three Aβ amyloid models.

REFERENCES

(1) Walsh, D. M., Lomakin, A., Benedek, G. B., Condron, M. M., and Teplow, D. (1997) Amyloid β-protein fibrillogenesis: detection of a protofibrillar intermediate. *J. Biol. Chem. 272*, 22364−22372.

(2) Kirkitadze, M. D., Bitan, G., and Teplow, D. B. (2002) Paradigm shifts in Alzheimer's Disease and other degenerative disorders: the emerging role of the oligomers assemblies. *J. Neurosci. Res. 69*, 567−577.

(3) Nostrand, W. E. V., Melchor, J. P., Cho, H. S., Greenberg, S. M., and Rebeck, G. W. (2001) Pathogenic Effects of D23N Iowa Mutant Amyloid β-Protein. *J. Biol. Chem. 276*, 32860−32866.

(4) Crescenzi, O., Tomaselli, S., Guerrini, R., Salvatori, S., D'Ursi, A. M., Temussi, P. A., and Picone, D. (2002) Solution structure of the Alzheimer amyloid β-peptide (1−42) in an apolar microenvironment. Similarity with a virus fusion domain. *Eur. J. Biochem. 269*, 5642−5648.

(5) Bitan, G., Kirkitadze, M. D., Lomakin, A., Vollers, S. S., Benedek, G. B., and Teplow, D. B. (2003) Amyloid β-protein (Aβ) assembly: Aβ40 and Aβ42 oligomerize through distinct pathways. *Proc. Natl. Acad. Sci. U.S.A. 100*, 330−335.

(6) Urbanc, B., Cruz, L., Yun, S., Buldyrev, S. V., Bitan, G., Teplow, D. B., and Stanley, H. E. (2004) *In silico* study of amyloid β-protein (Aβ) folding and oligomerization. *Proc. Natl. Acad. Sci. U.S.A. 101*, 17345−17350.

(7) Glabe, C. G. (2005) Amyloid accumulation and pathogensis of Alzheimer's disease: significance of monomeric, oligomeric and fibrillar Aβ. *Subcell Biochem. 38*, 167−177.

(8) Lazo, N. D., Grant, M. A., Condron, M. C., Rigby, A. C., and Teplow, D. B. (2005) On the nucleation of amyloid β-protein monomer folding. *Protein Sci. 14* (6), 1581−1596.

(9) Xu, Y., Shen, J., Luo, X., Zhu, W., Chen, K., Ma, J., and Jiang, H. (2005) Conformational transition of amyloid β-peptide. *Proc. Natl. Acad. Sci. U.S.A. 102*, 5403−5407.

(10) Baumketner, A., Bernstein, S. L., Wyttenbach, T., Bitan, G., Teplow, D. B., Bowers, M. T., and Shea, J.-E. (2006) Amyloid β-protein monomer structure: a computational and experimental study. *Protein Sci. 15*, 420−428.

(11) Lim, K. H., Collver, H. H., Le, Y. T. H., Nagchowdhuri, P., and Kenney, J. M. (2006) Characterization of distinct amyloidogenic conformations of the Aβ(1−40) and Aβ(1−42) peptides. *Biochem. Biophys. Res. Commun. 353*, 443−449.

(12) Teplow, D. B. (2006) Preparation of amyloid β-protein for structural and functional studies. *Methods Enzymol. 413*, 20−33.

(13) Grant, M. A., Lazo, N. D., Lomakin, A., Condron, M. M., Arai, H., Yamin, G., Rigby, A. C., and Teplow, D. B. (2007) Familial Alzheimer's disease mutations alter the stability of the amyloid β-protein monomer folding nucleus. *Proc. Natl. Acad. Sci. U.S.A. 104* (42), 16522−16527.

(14) Lam, A. R., Teplow, D. B., Stanley, H. E., and Urbanc, B. (2008) Effects of the Arctic (E^{22}→G) mutation on amyloid β-protein folding: discrete molecular dynamics study. *J. Am. Chem. Soc. 130*, 17413−17422.

(15) Hardy, J., and Selkoe, D. J. (2002) The amyloid hypothesis of Alzheimer's disease: progress and problems on the road to therapeutics. *Science 297*, 353−356.

(16) Hardy, J. (2002) Testing times for the "amyloid cascade hypothesis". *Neurobiol. Aging 23*, 1073−1074.

(17) Petkova, A. T., Ishii, Y., Balbach, J. J., Antzutkin, O. N., Leapman, R. D., Delaglio, F., and Tycko, R. (2002) A structural model for Alzheimer's β-amyloid fibrils based on experimental constraints from solid state NMR. *Proc. Natl. Acad. Sci. U.S.A. 99*, 16742−16747.

(18) Petkova, A. T., Yau, W. M., and Tycko, R. (2006) Experimental constraint on quaternary structure in Alzheimer's β-amyloid fibrils. *Biochemistry 45*, 598−512.

(19) Paravastu, A., Leapman, R. D., Yau, W. M., and Tycko, R. (2008) Molecular structural basis for polymorphism in Alzheimer's β-amyloid fibrils. *Proc. Natl. Acad. Sci. U.S.A. 105*, 18349−18354.

(20) Tycko, R., Sciarretta, K. L., Orgel, J. P. R. O., and Meredith, S. C. (2009) Evidence for novel β-sheet structures in Iowa mutant β-amyloid fibrils. *Biochemistry 48*, 6072−6084.

(21) Barrow, C. J., A., Y., Kenny, P. T. M., and Zagorski, M. G. (1992) Solution Conformations and Aggregational Properties of Synthetic Amyloid B-Peptides of Alzheimer's Disease: Analysis of Circular Dichroism Spectra. *J. Mol. Biol. 225*, 1075−1093.

(22) Gursky, O., and Aleshkov, S. (2000) Temperature-dependent β-sheet formation in beta-amyloid $Aβ_{1-40}$ peptide in water: uncoupling β-structure folding from aggregation. *Biochim. Biophys. Acta 1476*, 93−102.

(23) Frenkel, J. (1931) On the transformation of light into heat in solids. I. *Phys. Rev. 37*, 17−44.

(24) Besley, N. A., and Hirst, J. D. (1999) Theoretical studies toward quantitative protein circular dichroism calculations. *J. Am. Chem. Soc. 121*, 9636−9644.

(25) Woody, R. W. (2005) The exciton model and the circular dichroism of polypeptides. *Monatsh. Chem. 136*, 347−366.

(26) Bulheller, B. M., Rodger, A., and Hirst, J. D. (2007) Circular and linear dichroism of proteins. *Phys. Chem. Chem. Phys. 9*, 2020−2035.

(27) Abramavicius, D., Palmieri, B., Voronine, D. V., Sanda, F., and Mukamel, S. (2009) Coherent multidimensional optical spectroscopy of excitons in molecular aggregates; quasiparticle versus supermolecule perspectives. *Chem. Rev. 109*, 2350−2408.

(28) Smith, A. W., and Tokmakoff, A. (2007) Amide I two-dimensional infrared spectroscopy of β-hairpin peptides. *J. Chem. Phys. 125*, 045109−1−10.

(29) Kim, Y. S., Liu, L., Axelsen, P. H., and Hochstrasser, R. M. (2008) Two-dimensional infrared spectra of isotopically diluted amyloid fibrils from Aβ40. *Proc. Natl. Acad. Sci. U.S.A. 105*, 7720−7725.

(30) Strasfeld, D. B., Ling, Y. L., Shim, S.-H., and Zanni, M. T. (2008) Tracking fiber formation in human islet amyloid polypeptide with automated 2D-IR spectroscopy. *J. Am. Chem. Soc. 130*, 6698−6699.

(31) Shim, S.-H., Gupta, R., Ling, Y. L., Strasfeld, D. B., Raleigh, D. P., and Zanni, M. T. (2009) Two-dimensional IR spectroscopy and isotope labeling defines the pathway of amyloid formation with residue-specific resolution. *Proc. Natl. Acad. Sci. U.S.A. 106*, 6614−6619.

(32) Jiang, J., Abramavicius, D., Bulheller, B. M., Hirst, J. D., and Mukamel, S. (2010) Ultraviolet spectroscopy of protein backbone

transitions in aqueous solution: combined QM and MM simulations. *J. Phys. Chem. B 114*, 8270−8277.
(33) Jiang, J., and Mukamel, S. (2010) Two-dimensional ultraviolet (2DUV) spectroscopic tools for identifying fibrillation propensity of protein residue sequences. *Angew. Chem. 49*, 9666−9669.
(34) Jiang, J., and Mukamel, S. (2011) Two-dimensional near-ultraviolet spectroscopy of aromatic residues in amyloid fibrils: a first principles study. *Phys. Chem. Chem. Phys. 13*, 2394−2400.
(35) Phillips, J. C., R. Braun, W. W., Gumbart, J., Tajkhorshid, E., Villa, E., Chipot, C., Skeel, R. D., Kalé, L., and Schulten, K. (2005) Scalable molecular dynamics with NAMD. *J. Comput. Chem. 26* (16), 1781−1802.
(36) MacKerell, A. D., et al. (1998) All-atom empirical potential for molecular modeling and dynamics studies of proteins. *J. Comput. Chem. 102*, 3586−3616.
(37) Jiang, J., Abramavicius, D., Falvo, C., Bulheller, B. M., Hirst, J. D., and Mukamel, S. (2010) Simulation of two dimensional ultraviolet (2DUV) spectroscopy of amyloid fibrils. *J. Phys. Chem. B 114*, 12150−12156.
(38) Zhuang, W., Abramavicius, D., and Mukamel, S. (2005) Dissecting coherent vibrational spectra of small proteins into secondary structural elements by sensitivity analysis. *Proc. Natl. Acad. Sci. U.S.A. 102* (7), 7443−7448.
(39) Jiang, J., and Mukamel, S. (2011) Probing amyloid fibril growth by two-dimensional near-ultraviolet spectroscopy. *J. Phys. Chem. B 115*, 6321−6328.
(40) Van Nostrand, W. E., Melchor, J. P., and Ruffini, L. (1998) Pathologic amyloid β-protein cell surface fibril assembly on cultured human cerebrovascular smooth muscle cells. *J. Neurochem. 70*, 216−223.